Supplementary Information for

Emergence of Dynamic G-Tetraplex Scaffold: Uncovering Low Salt-Induced Conformational Heterogeneity and Folding Mechanism

Manali Basu[1, 2, †], Avijit Mainan[3,†], Susmita Roy[3,*], Padmaja Prasad Mishra[1,2,*]

[1]Single Molecule Biophysics Lab, Chemical Sciences Division,
Saha Institute of Nuclear Physics,
1/AF Bidhannagar, Kolkata 700064, India
[2]Homi Bhabha National Institute, Mumbai
E-mail: padmaja.mishra@saha.ac.in

[3]Department of Chemical Sciences
Indian Institute of Science Education and Research Kolkata,
Mohanpur Campus, Nadia, West Bengal 741246, India
Email: susmita.roy@iiserkol.ac.in

[†]This authors have equal contribution

*Corresponding Author

Details of SBM Potential

V_{SBM} is the all-atom structure-based model potential which ensures the global minimum in the energy landscape for DNA native state. V_{SBM} can be separated into local and non-local interactions. Restrained harmonic potential for bonds, angles, improper/planer, and proper/flexible dihedral angles are described as local interaction. The non-local term is stated with Lennard Jones' 6-12 potential for close interactions defined as contact-pair present in the native NMR structure whereas the non-native pairs are treated as repulsive.

$$V_{SBM} = V_{SBM,local} + V_{SBM,non-local} \quad \text{(Eq. S1)}$$

$$V_{SBM,local} = \sum_{i}^{bonds} \frac{\beta_r}{2}\left(r_i - r_i^0\right)^2 + \sum_{i}^{angles} \frac{\beta_\theta}{2}\left(\theta_i - \theta_i^0\right)^2 + \sum_{i}^{improper/planner} \frac{\beta_\chi}{2}\left(\chi_i - \chi_i^0\right)^2 + \sum_{i}^{\substack{proper \\ dihedrals}} \beta_\phi F_D\left(\phi_i - \phi_i^0\right) \quad \text{(Eq. S2)}$$

$$\text{where, } F_D(\phi) = [1 - \cos(\phi)] + \frac{1}{2}[1 - \cos(3\phi)] \quad \text{(Eq. S3)}$$

$$V_{SBM,non-local} = \sum_{ij}^{contacts} \beta_C \left(\left(\frac{\sigma_{ij}}{r_{ij}}\right)^{12} - 2\left(\frac{\sigma_{ij}}{r_{ij}}\right)^{6}\right) + \sum_{ij}^{non-contacts} \beta_{NC}\left(\frac{\sigma_{NC}}{r_{ij}}\right)^{12} \quad \text{(Eq. S4)}$$

All initial geometric parameters $(r_i^0, \theta_i^0, \chi_i^0, \phi_i^0, \sigma_{ij})$ are received from the NMR structure. Total contact energy to dihedral energy ratio is conserved as, $\sum_i^{contacts} \beta_C \,/ \sum_i^{\substack{proper \\ dihedrals}} \beta_\phi = 2$. Contact pairs are calculated using the Shadow Algorithm.

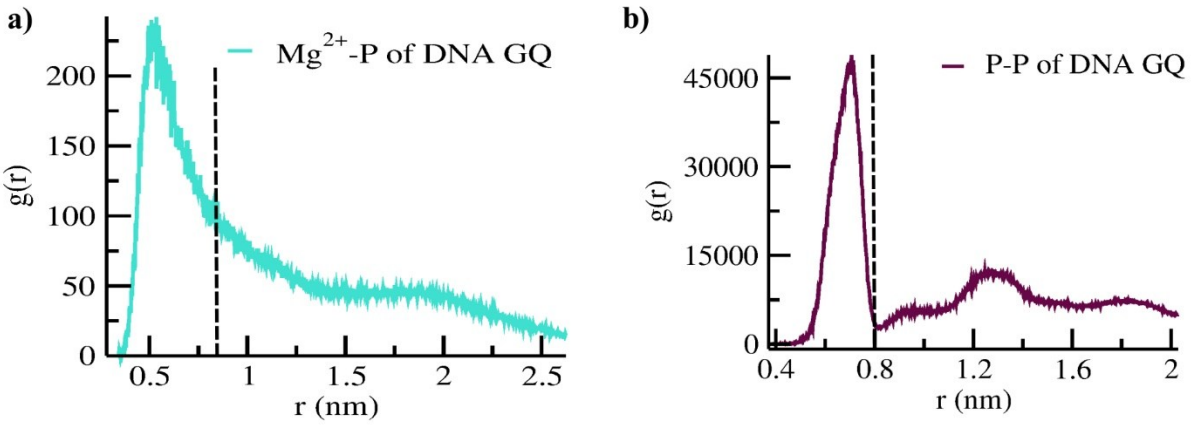

Figure S1: Radial distribution function (RDF) plots are used to establish cut-off distances for calculating Mg^{2+} site visiting frequency and Mg^{2+}-mediated contact maps. (a) RDF of Mg^{2+} ions around the phosphate group of DNA, with the boundary indicated for determining the site visiting frequency of Mg^{2+} ions. (b) RDF between phosphate groups within the DNA, with the highlighted boundary serving as the cut-off distance for calculating the Mg^{2+}-mediated contact map.

Table S1: The cut-off distances for average Mg^{2+} ion condensation and Mg^{2+}-mediated contact map.

Contact Map types	**Cut-off $_{Mg^{2+}\text{-}P}$ (nm)**	**Cut-off $_{P\text{-}P}$ (nm)**
Average Mg^{2+} ion condensation ($\theta_{Mg^{2+}}$)	0.85	Not applicable
Mg^{2+}-mediated contact map	0.85	0.8

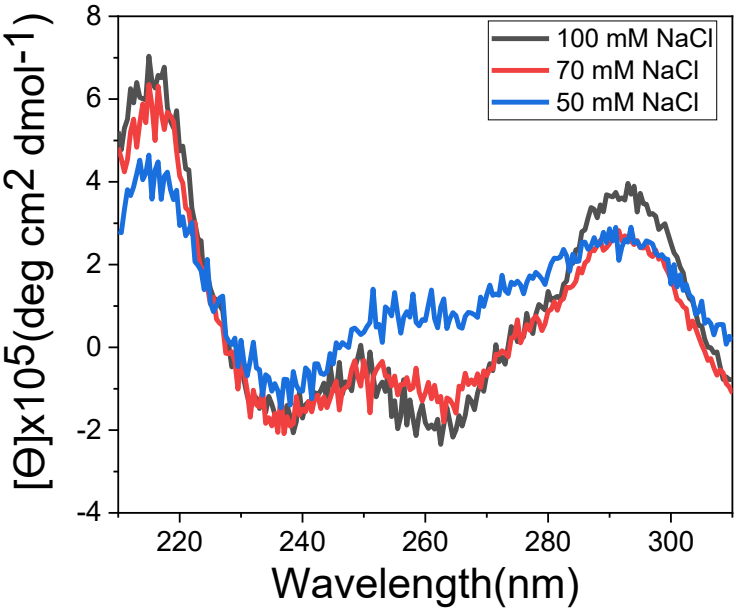

Figure S2: CD spectra of telomeric DNA in a 20 mM Tris buffer at various NaCl concentrations at 25 °C.

Table S2: Distance between the two ends of the G-quadruplex corresponding to FRET efficiency values at various concentrations of NaCl.

Conc. Of NaCl	FRET States	Distance between Cy3 and Cy5 (nm)
50 mM NaCl	0.19 0.44 0.73	8.13 7.25 6.87
70 mM NaCl	0.24 0.51 0.70	7.88 7.18 6.90
100 mM NaCl	0.27 0.51 0.74	7.74 7.17 6.91

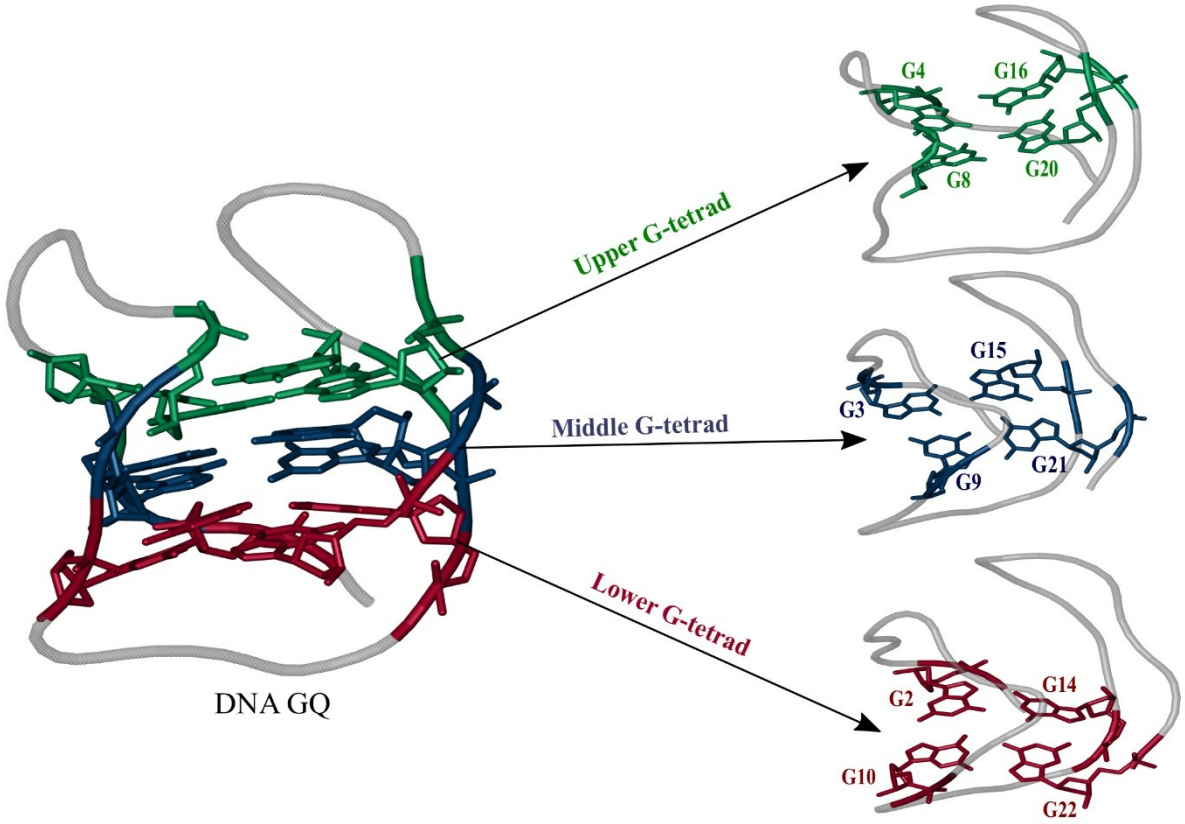

Figure S3: DNA G-quadruplex structure featuring three G-tetrad planes: the lower plane includes G2-G10-G14-G22, the middle plane consists of G3-G19-G15-G21 and the upper plane is composed of G4-G8-G16-G20.

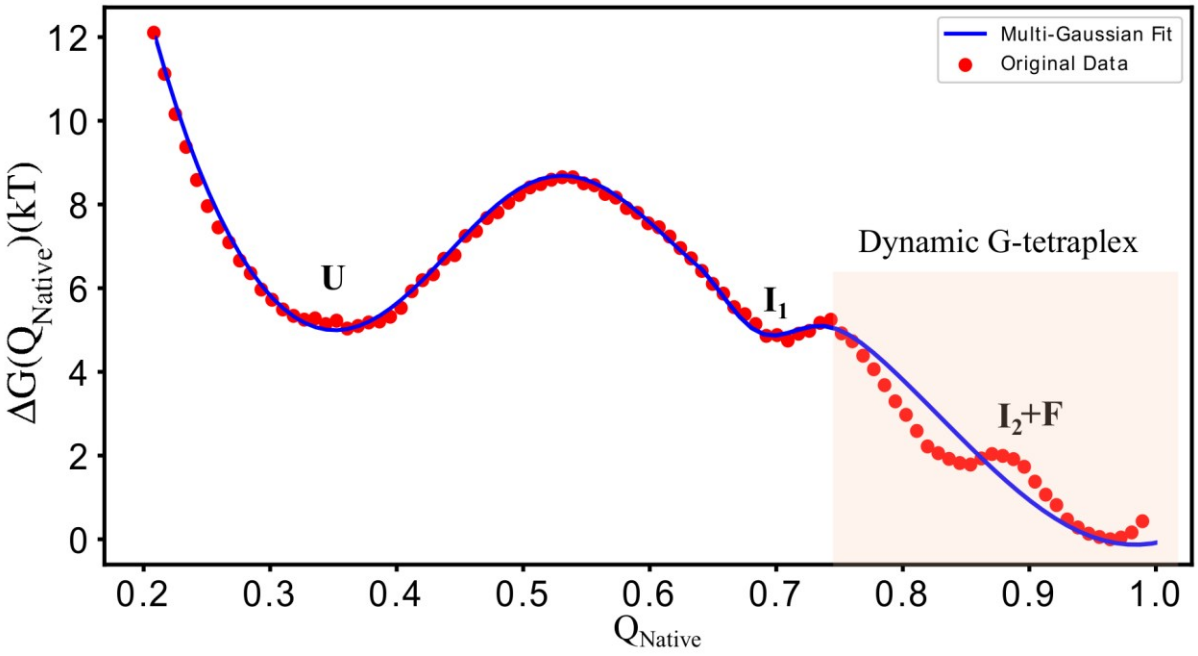

Figure S4: Transition from a four-state to a three-state model of free energy profile, where states I_2 and F merge into a dynamic G-tetraplex state.

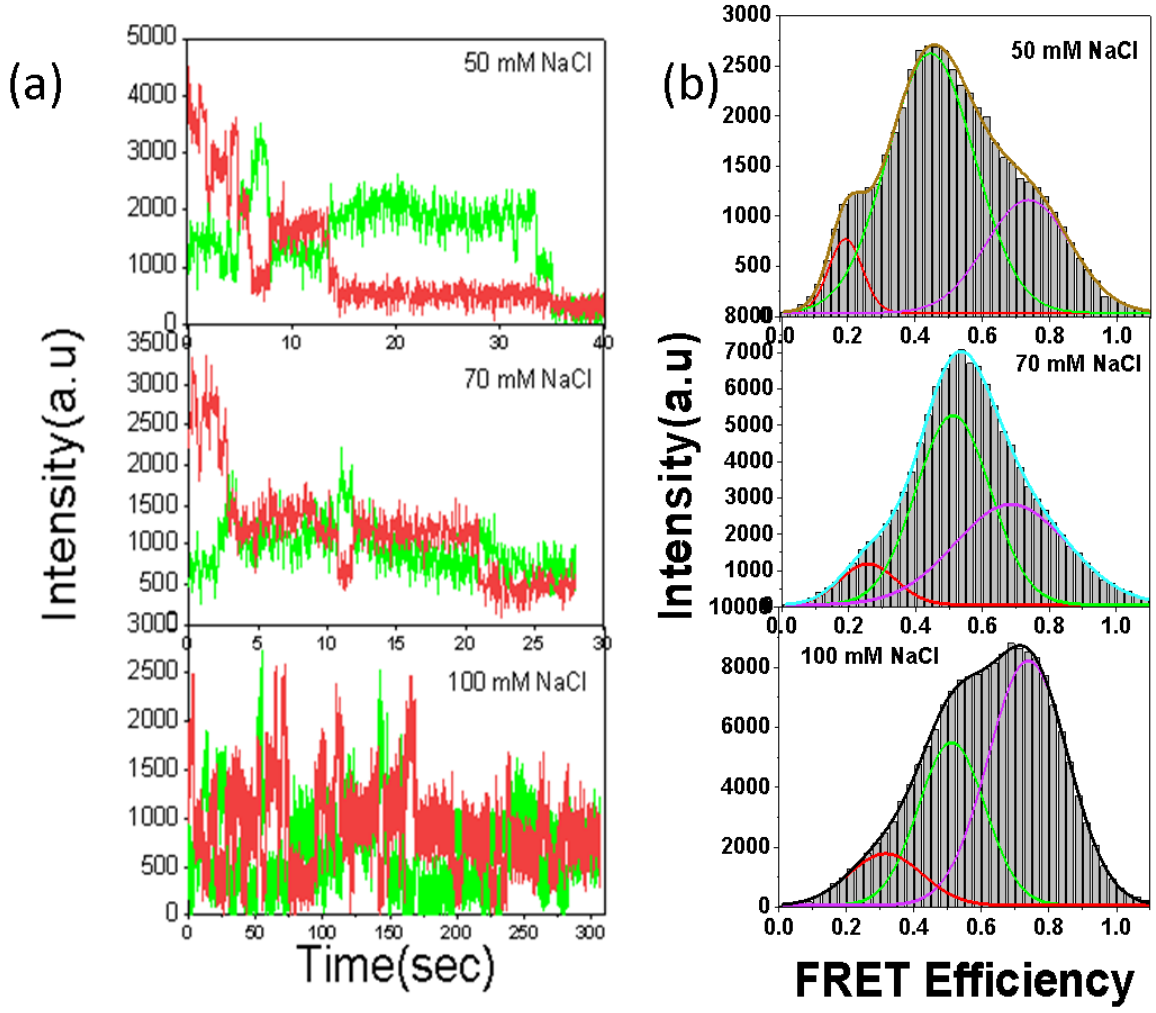

Figure S5: Representative single-molecule FRET traces and unnormalized histograms at various concentrations of NaCl

Table S3: Comparison of the area under the curve from single-molecule FRET and atomistic STEM simulation results show the normalized population of the dynamic G-tetraplex state at different NaCl concentrations.

Concentration of NaCl	smFRET Peak Positions (High)	Area under the Curve (smFRET)	Area under the Curve (STEM Simulation)
50 mM	0.75	13.25	0.807
70 mM	0.70	16.48	0.878
100 mM	0.73	27.52	0.992

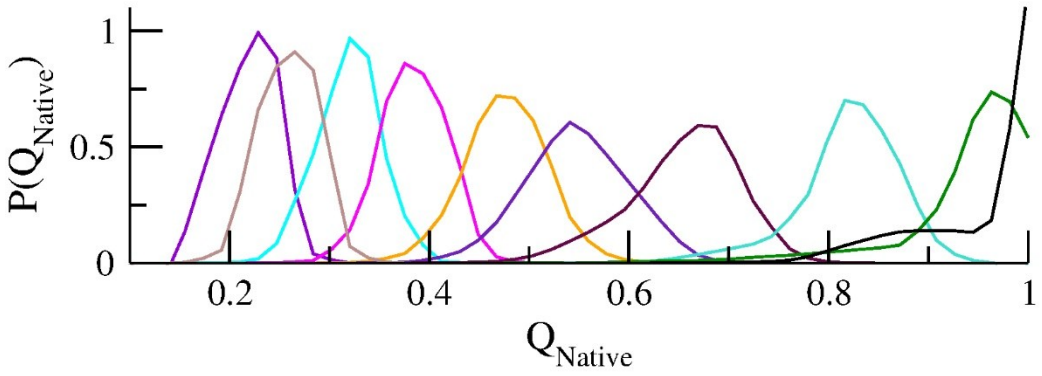

Figure S6: The overlap of conformational space in the neighboring windows as a histogram plot. 10 windows are used where the fraction of global native contacts (Q_{Native}) varies from 0.14 to 1 and is represented as unfolded (U) to folded (F) state respectively. The probability distribution of Q_{Native} shows an ideal overlap of the configuration.